Sampling Report: BR05DD01, Ooramina-1 and Wallara-1

Amber J. M. Jarrett and Jochen Brocks

Research School of Earth Sciences, Australian National University

ABSTRACT: This report contains the results and interpretations of a sampling study of drillcores BR05DD01, Ooramina-1 and Wallara-1 was undertaken in 2010 and 2012. We provide new insights into redox conditions in the Neoproterozoic of Australia, and ancient microbial systems from pre-Sturtian and the inter-Snowball periods in times previously absent in the global record.

1. Introduction

The Neoproterozoic was a time of rampant diversification of eukaryotes from single celled organisms to complex animals. However, the causes of this diversification are still not clear. It has been suggested that a rise in atmospheric oxygenation was a defining catalyst. This is consistent with the observation that the Neoproterozoic was also a time of transition to well-oxygenated deep marine waters from the stratified and anoxic water masses which dominated Earth's middle age. However, oxygenation of deep waters is strongly diachronous on different continents and in different basins. To date, there has been no study looking at the relationships between ocean chemistry and eukaryote evolution in Australia.

As a result of the economical petroleum potential of the Amadeus Bain, there have been many studies examining the hydrocarbon (HC) composition, the gas and oil potential of both Phanerozoic and Neoproterozoic carbonates and shales (Jackson *et al.* 1984; Marshall *et al.* 2008) and to research the evolution of life, including steranes as proxies for eukaryotes though the Neoproterozoic (e.g. Logan *et al.* 1999; Summons and Powell 1991).

In previous published studies before the extent of the potential of contamination was fully appreciated, rock samples did not have their exterior surfaces removed prior to analysis, nor were they tested for their susceptibility to hydrocarbon infiltration. Neoproterozoic shales

with low TOC are significantly susceptible to overprinting from contaminant molecules (Brocks *et al.* 2008). Summons & Powell (1991) describe sterane patterns in the Pertatataka Formation and Bitter Springs Formation that, quote by the authors, '*look marine and Mesozoic or Tertiary*' (p 521) suggesting that the steranes could possibly be younger anthropogenic contaminants. In addition, Summons & Powell (1991) demonstrated that the Neoproterozoic Pertatataka and Bitter Springs Formations contain very low TOC rocks, the majority under 1 % TOC (Summons & Powell, 1991). We hypothesise that the low TOC of these rocks, plus the potential of HC contamination during drilling and storage could mean that there are few published data points from the Amadeus Basin likely not tainted by anthropogenic hydrocarbons.

Samples were collected from the Alice Springs drillcore store to answer three major questions;

1. What was the redox state of the Amadeus Basin in the Neoproterozoic?
2. Were previously published biomarker results influenced by petroleum contamination? and if so
3. What is the indigenous sterane signature of the Neoproterozoic?
4. What is the relationship between oxygen and evolution in the Neoproterozoic Amadeus Basin, central Australia?

The redox state of the Amadeus Basin was characterised using iron (Fe) speciation techniques including sequential Fe and pyrite extraction as described in detail by Poulton & Canfield (2005) and below. Biomarker contamination was assessed by removing the exterior portion of a rock and quantitatively analysing hydrocarbons in the exterior and interior portions. This method has been described in detail by Brocks *et al.* (2008) and Jarrett *et al.* 2013 and below.

2. Sample collection and methodologies

Samples were collected from BR05DD01, Ooramina-1 and Wallara-1 and in September 2009 and May 2012 and were subjected to inorganic and organic techniques (Table 1).

Table 1. Techniques used on the three drillcores

	BR05DD01	Ooramina-1	Wallara-1
Fe Speciation	X	X	✓
XRF	✓	X	✓
Biomarkers	✓	✓	✓

2.1 Sequential Fe extraction

Fe speciation analysis was conducted using sequential methods described by Poulton & Canfield (2005), which recognise and extract different operationally-defined pools of Fe. Carbonate Fe (Fe_{Carb}) bound in minerals such as siderite and ankerite was extracted from *ca.* 100 mg of powdered rock with 10 ml of 1 M sodium acetate adjusted to pH 4.5 for 48 h at 50°C. Fe from reducible oxides (Fe_{Ox}) such as goethite and hematite was extracted using a sodium dithionite solution buffered to pH 4.8 with 0.35 M acetic acid and 0.2 M sodium citrate for 2 h. Magnetite (Fe_{Mag}) was extracted with 10 ml of a 0.2 M ammonium oxalate and 0.17 M oxalic acid solution for 6 h. Total Fe was extracted from ca. 100 mg ashed (550°C, 12 h) sample using HF-$HClO_4$-HNO_3. All Fe extracts were analysed by atomic absorption spectrometry (AAS) using a Varian Spectra AA 400.

2.2 Pyrite extraction

Pyrite (Fe_{Py}) was extracted in a 2 M chromous chloride solution followed by precipitation of the released hydrogen sulfide as Ag_2S (Canfield *et al.,* 1986). The Fe content was calculated gravimetrically assuming pyrite stoichiometry (FeS_2). Replicate analyses gave a reproducibility of < ± 5% for all extractions. The sum of the sequential extraction steps plus pyrite (i.e., Fe_{Carb} + Fe_{Ox} + Fe_{Mag} + Fe_{Py}) defines an iron pool that is considered highly reactive (Fe_{HR}) towards reductive dissolution during deposition and early diagenesis (Poulton & Canfield, 2005).

2.3 Removal of exterior surfaces for biomarker analyses

Two methods were used to remove the exterior surfaces of a rock. The surfaces of large and compact rocks were trimmed using a precision saw (Buehler Isomet™ 1000; Illinois, U.S.A). Prior to use, the blade and sample holder were cleaned with methanol and dichloromethane (DCM; solvent grade 99.9%, UltimAR®, Mallinckrodt Chemicals). Distilled water was used as the lubricant. Between each cut the saw blade was solvent cleaned and distilled water was changed. All surfaces of the drillcores were cut as described by Brocks *et al.* (2008).

The second method, micro-ablation is used on small or fissile rocks which cannot be sawed (Jarrett *et al.* 2013). The apparatus is composed of a KG-1 Mini-Sonic tumbler (Diamond Pacific, USA), modified so that all components in contact with rock samples can be cleaned by combustion at 600°C . The Mini-Sonic tumbler transmits vibrational energy to the hopper at a frequency of > 3,500 per minute (Jarrett *et al.* 2013).

2.4 Extraction of bitumen

Bitumen was extracted from the rock powder with a Dionex Accelerated Solvent Extractor (ASE 200) using 90% DCM and 10% methanol. The solvent extracts were reduced to 100 µl under a stream of pure nitrogen gas (N_2). The molecules were then fractionated into saturate, aromatic, and polar fractions using micro column chromatography over annealed and dry packed silica gel. Saturate hydrocarbons were eluted with 0.5 dead volumes (DV) of *n*-hexane, aromatic hydrocarbons with 2 DV of *n*-hexane:DCM (1:1 v/v) and polars with 3 DV DCM:methanol (1:1 v/v). An internal standard 18-MEAME (18-methyl-eicosanoic acid methyl-ester; Chiron Laboratories AS), was added to the saturated and aromatic fractions (2 µg), while 50 ng of D4 (d4-C29-ααα-ethylcholestane; Chiron Laboratories AS) was added to the saturated fraction only. Extracts were then evaluated and biomarkers quantified using GC-MS.

2.5 Gas Chromatography- Mass Spectrometry (GC-MS)

GC-MS analyses were carried out on an Agilent 6890 gas chromatograph (GC) coupled to a Micromass Autospec Premier double sector mass spectrometer (MS). The GC was equipped with a 60 m DB-5 capillary column (0.25 mm i.d., 0.25 µm film thickness) and helium was used as the carrier gas at a constant flow of 1 ml/min. The MS source was operated at 260˚C in EI mode at 70 eV ionisation energy and 8000 V acceleration voltage. For full analysis of the hydrocarbon samples, four GC-MS runs are needed: full scan at 1000 mass resolution of both the saturated and aromatic fractions, selected ion recording (SIR) of the aromatic hydrocarbon fraction and metastable reaction monitoring (MRM) to determine sterane and hopane biomarker concentrations in the saturate fraction.

3. Results & Discussion

3.1 Fe speciation and the redox state of the Amadeus Basin

The results for Fe speciation in drillcore Wallara-1 is presented in Figure 1, raw data is presented in Appendix 1 and the paleoredox state of each formation is described below.

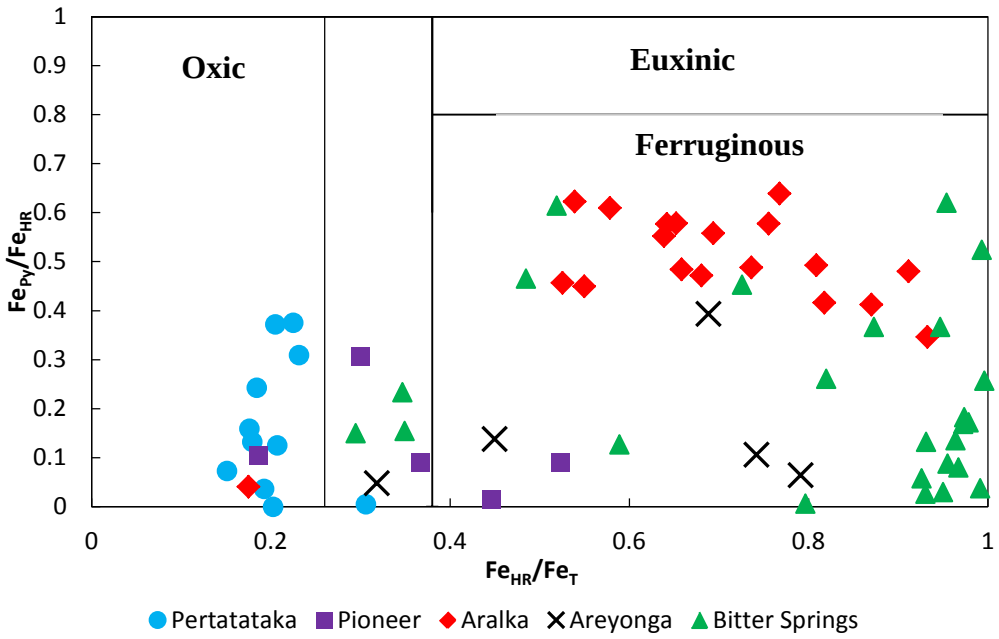

Figure 1. A cross plot of Fe_{Py}/Fe_{HR} versus Fe_{HR}/Fe_T summarising the changes in Fe speciation through Wallara-1. Regions of water column redox chemistry are based on Poulton & Canfield (2011).

3.1.1 The Bitter Springs Formation

Carbonate sediments of the Bitter Springs formation contain low concentrations of Fe with the majority in the highly reactive phase (Figure 1). Fe_{HR}/Fe_T values are scattered and variable (Figure 1). At the time of deposition *ca.* 820 Ma the atmosphere would have been at least weakly oxygenated (Shields-Zhou and Och, 2011). As these sediments were deposited in relatively shallow water, water-atmosphere interactions would have affected Fe_{HR}/Fe_T (Canfield *et al.* 2008). The majority of samples analysed from the Bitter Springs Formation were taken from samples that were not oxidised or red. This is a dominant feature of the JCM and parts of the LCM. Therefore, the results may be skewed towards anoxia, when there is clear evidence of a partially oxidised system.

3.1.2 Areyonga diamictite

The Areyonga diamictite provides an insight into sediments transported into the ocean during, and/or immediately after the Sturtian glaciation. The ratio of Fe_{HR}/Fe_T, on average is lower than in the Bitter Springs Formation (Figure 1) likely due to the influx of unreactive iron silicates brought into the system as glacial flour and clasts. Fe speciation indicates that the Areyonga diamictite was deposited under largely anoxic and ferruginous conditions (Figure 1). This is consistent with theoretical modelling of redox conditions through glacial conditions (Canfield and Raiswell, 1999; Hoffman *et al.* 2011).

3.1.3 Aralka Formation

The Aralka formation exhibits an excursion of Fe_T, largely due to an increase in pyrite (Figure 1). Fe_{Py}/Fe_{HR} never exceeds 0.8 throughout the entire core, including the increase in the Aralka Formation (Figure 4.5), indicating that the water column in the Aralka remained ferruginous, and never became euxinic.

3.1.4 Pioneer Sandstone

Data points for the Pioneer sandstone are few (*n* = 5) and therefore a detailed assessment of the Marinoan glacial outwash deposit cannot be made with certainty. The sandstone contains less Fe than the Aralka Formation likely due to quartz dilution (Lyons and Severmann, 2006). Fe speciation signals are mixed and may suggest an anoxic mid to deep shelf water column at the time of deposition after the Marinoan Glaciation (Figure 1; Lyons & Severmann, 2006). Due to the high quartz content, an assessment of redox during the deposition of the Pioneer is currently impossible based on Fe speciation alone.

3.1.5 Pertatataka Formation

The Pertatataka Formation contains Fe speciation results suggestive of an oxygenated water column (Figure 1). Moreover, redox chemistry is stable with Fe_{HR}/Fe_T values oscillating around $0.20^{0.17}_{0.23}$ (95% confidence interval). Therefore, the results of this study demonstrate that the post Marinoan deeper water environment of Australia was stably, and persistently oxic. More samples from the Centralian Superbasin need to be analysed for consistency, especially sediments which include the Olympic Formation, the diamictite correlative to the Pioneer Sandstone in addition to other sections that record a conformable transition from

the Pioneer Sandstone or Olympic Formation to the Pertatataka Formation to test whether Ediacaran oxygenation in Australia encompassed the entire basin.

3.2 Contamination in the Amadeus Basin

It is crucial in ancient and organically lean samples to determine whether hydrocarbons (HCs) extracted from a rock are allochthonous, or were introduced during the drilling, sampling or storage processes. At the NTGS drillcore storage facilities in Darwin and Alice Springs NT, BR05DD01 was placed on orange plastic liners inside metal trays. In Darwin, the trays were stored in a partially open warehouse and in both Darwin and Alice Springs the cores were partly covered with a fine layer of red dust. These have been shown in the past to contain contaminants that can influence the hydrocarbon signature of a rock.

3.2.1 HCs in the core liner and dust

GC-MS results indicate that both the core liner and dust contained significant amounts of hydrocarbons (HCs) (Figures 2 and 3).

Core liner contaminants

The core liner contains a series of *n*-alkanes ranging from C_{15} to C_{34} with concentrations ranging from 0.05 – 0.4 µg / g with a total n-alkane concentration of 1.65 µg / g (Figure 2). Low molecular weight (MW) *n*-alkanes (≤ *n*-C_{20}) are in high concentration with a sharp drop off after *n*-C_{20}. High MW *n*-alkanes (> *n*-C_{20}) are present with an even-over-odd carbon number preference *n*-C_{20} to *n*-C_{30}. Alkyl cyclopentanes are also present in the core liner with an even numbered carbon preference in the range C_{15} – C_{23} (Cyclopentane carbone preference index, CP-CPI = 6.37; CP-CPI is defined in Brocks *et al.* 2008) (Figure 2). Five series of BAQCs known to derive from polyethylene (PE) were also identified in the core liner; 3-3,-diethylalkanes (DEAs), 5,5-DEAs, 6,6-DEAs, 5-butyl, 5-ethylalkanes and 6-butyl, 6-ethylalkanes. These molecules were identified using the *m*/*z* 99, 127-113, 141-127, 155-141 and 169-155 traces respectively. Methylalkanes and dimethylalkanes are also present and have similar distributions to those described from polyethylene (PE) by Grosjean & Logan (2007) and Brocks *et al.* (2008). HCs derived from PE have been shown to infiltrate drillcore material thus compromising potential indigenous HC distributions (Brocks *et al.* 2008; Grosjean and Logan 2007).

Dust contaminants

The GC-MS fullscan of red dust extract is presented in Figure 3 and indicates significant amounts of HCs. The dust contains a bimodal *n*-alkane envelope ranging from *n*-C_{15} to *n*-C_{38} (Figure 6.3). Concentrations of individual *n*-alkanes range from 0.002 – 0.3 µg / g dust with a large UCM probably indicating bio-degradation. *n*-alkanes in the range *n*-C_{15} to *n*-C_{24} have even-over-odd carbon-numbered predominance, with a maximum at *n*-C_{18}. *n*-alkanes in the range *n*-C_{25} to *n*-C_{37} have an odd-over-even carbon-numbered predominance, with *n*-C_{31} in the highest concentration (Figure 3). High molecular weight *n*-alkanes > C_{25} with odd-over-even predominance can be sourced from plant leaf waxes, which is often a major constituent of dust (Rogge *et al.* 2006). The dust also contains hydrocarbons such as the isoprenoids pristane and phytane, in addition to steranes and hopanes. The angiosperm triterpenoids oleanane and taraxastane are also present.

Hydrocarbons have also been identified in dust in other locations. Marynowski *et al.* 2004 suggest that steranes and homohopanes in the dust from the Upper Silesia, Poland reflect petroleum based input from diesel exhaust fumes, or paved road dust. Rogge *et al.* (1993) characterised road dust and found traces of petroleum based diesel fumes and tyre debris. The drillcore facility in Darwin contains forklifts running on gas, in addition to a number of petroleum based generators on site. Furthermore, the drillcore shed is open to the elements and is in close proximity to the air base and a major highway providing additional opportunities for petroleum based contamination of the drillcore. The core may also have been exposed to exhaust fumes at the drilling site, or during transport to the facility (Brocks *et al.* 2003).

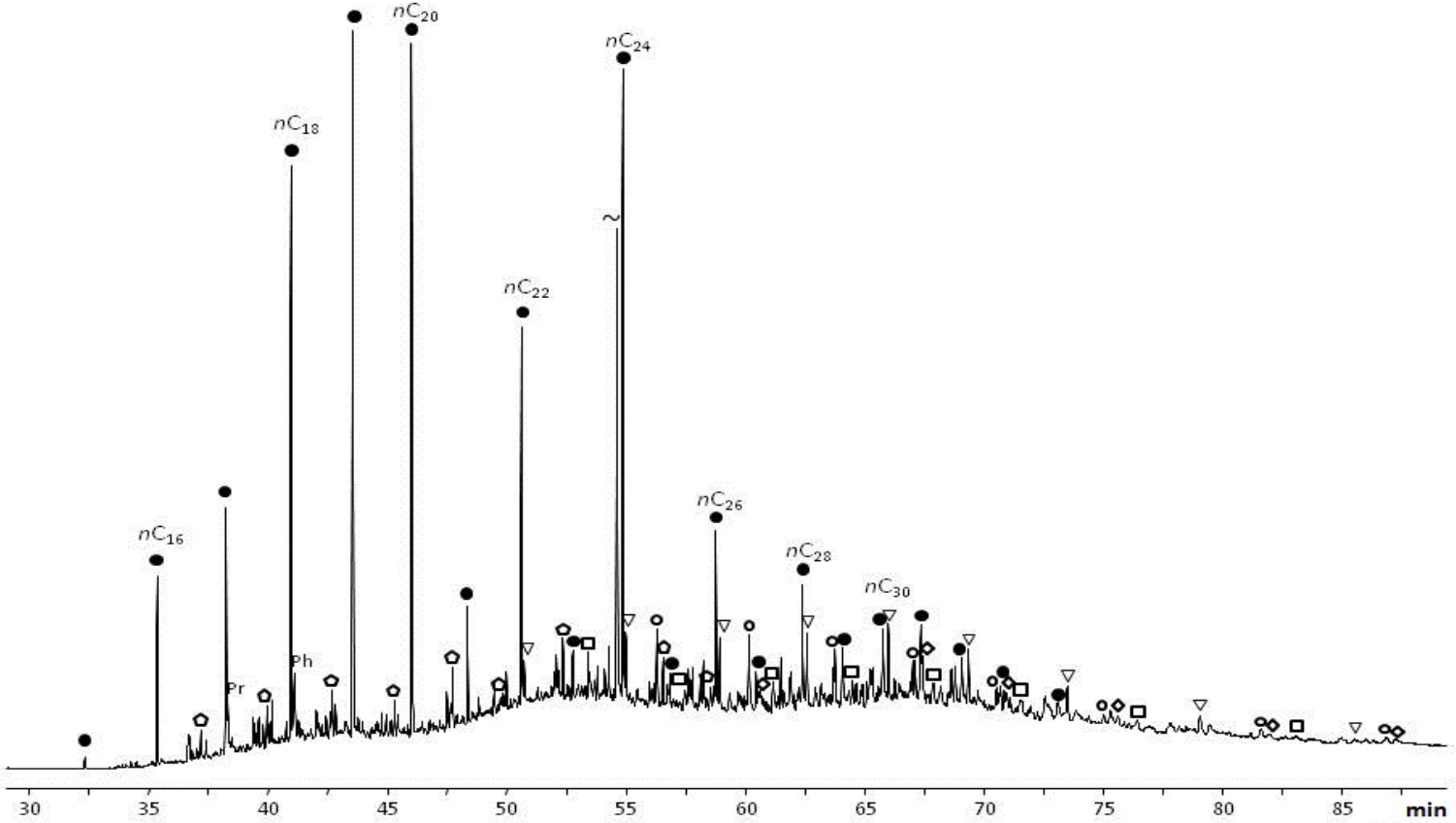

Figure 2. GC-MS full scan chromatogram of the extracted saturated hydrocarbons in the core liner. Filled circles = *n*-alkanes, pentagons = cyclopentyl alkanes, open circles = 3,3-DEAs, open triangles = 5,5-DEAs, squares = 6,6-DEAs, and ~ = truncated 18-MEAME standard.

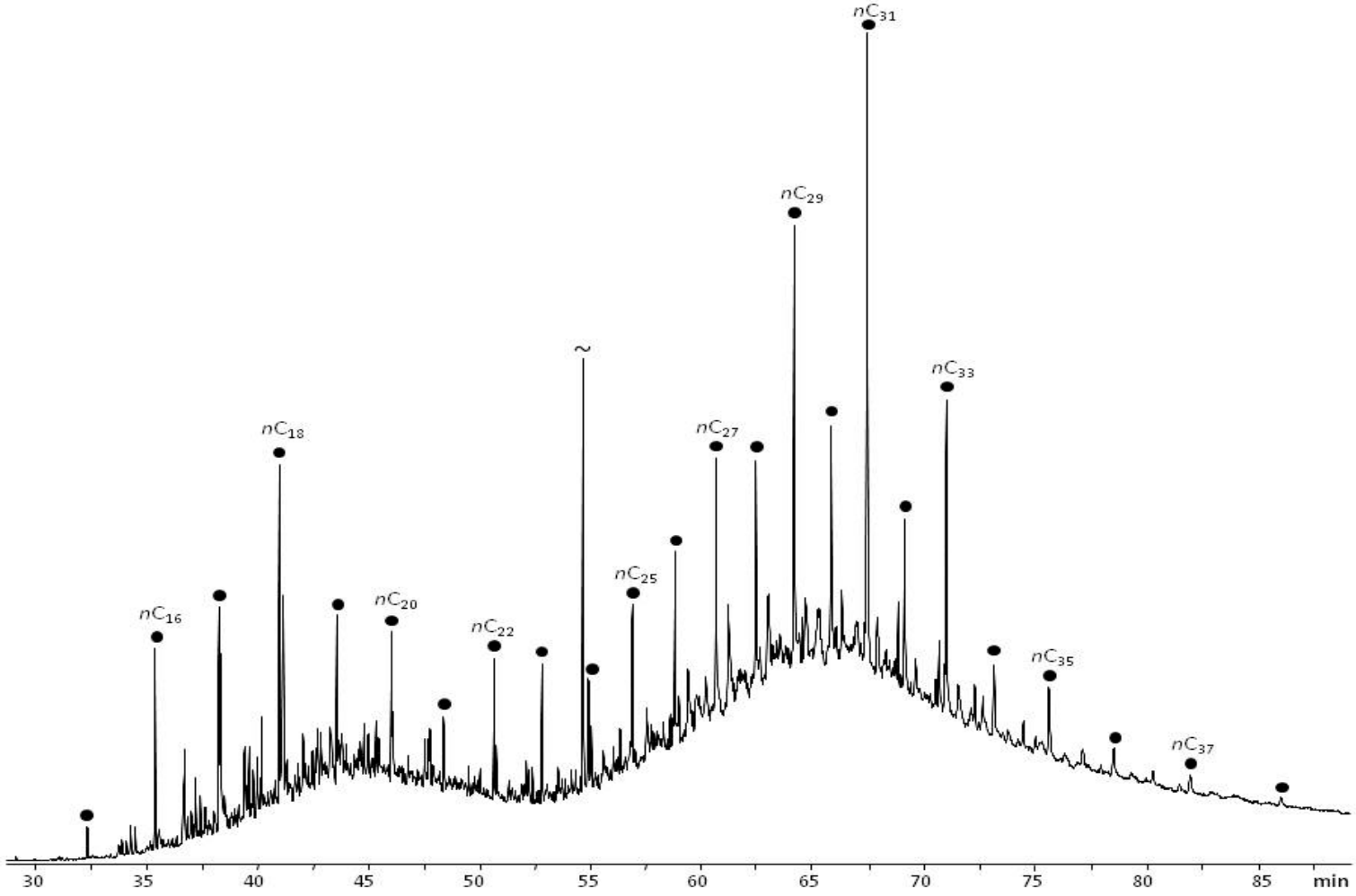

Figure 3. GC-MS full scan chromatogram of the extracted saturated hydrocarbons in the dust found at the bottom of the core tray. Filled circles = *n*-alkanes and ~ = truncates the 18-MEAME standard.

3.2.2 Exterior/interior (E/I) ratios

E/I ratios were calculated for *n*-alkanes, steranes and hopanes in drillcores BR05DD01 and Wallara-1 to determine whether they are allochthonous or indigenous and are presented in Appendicies 3 and 4. Only one sample from drillcore Ooramina-1 was analysed in this study and was found to be devoid of indigenous biomarkers and excluded from further analyses. Furthermore, the extracts from the drillcores were compared to the core liner and dust extracts to determine whether there was any evidence of surficial contamination. Surficial contamination can be recognised by elevated E/I ratios, while indigenous HCs will commonly yield E/I ≈ 1 ±0.2 to include potential integration error and evaporation from exterior surfaces.

E/I ratios indicate that the majority of samples contain higher concentrations of *n*-alkanes on the surfaces, three of these contained *n*-alkanes on the exterior although they were below detection limits in the interior. Differences in E/I ratios, particularly those < 1, are clearly due to evaporation of HCs from rock surfaces, possibly due to the high temperatures (average *ca.* 30°C) in Alice Springs and Darwin.

An example for high sterane E/I is sample 471.50 m (Figure 4). This sample has *n*-alkane and hopane E/I ratios ≈ 1, however steranes are *ca.* 8 times higher on the exterior (Appendix 2). MRM results indicate that only the C_{27} sterane is present in the interior fraction, while all three sterane homologues are present in the exterior fraction (Figure 4). All rocks in the same formation, above and below 471.50 m with sterane E/I ≈ 1 only contains C_{27} in both fractions. Therefore, the exterior of 471.50 m has been tainted with petroleum based contaminants containing several sterane pseudo homologues, where the C_{27} sterane is indigenous. This same trend is also evident in Wallara-1 where all samples identified were either devoid of HCs or thoroughly contaminated (Figure 5).

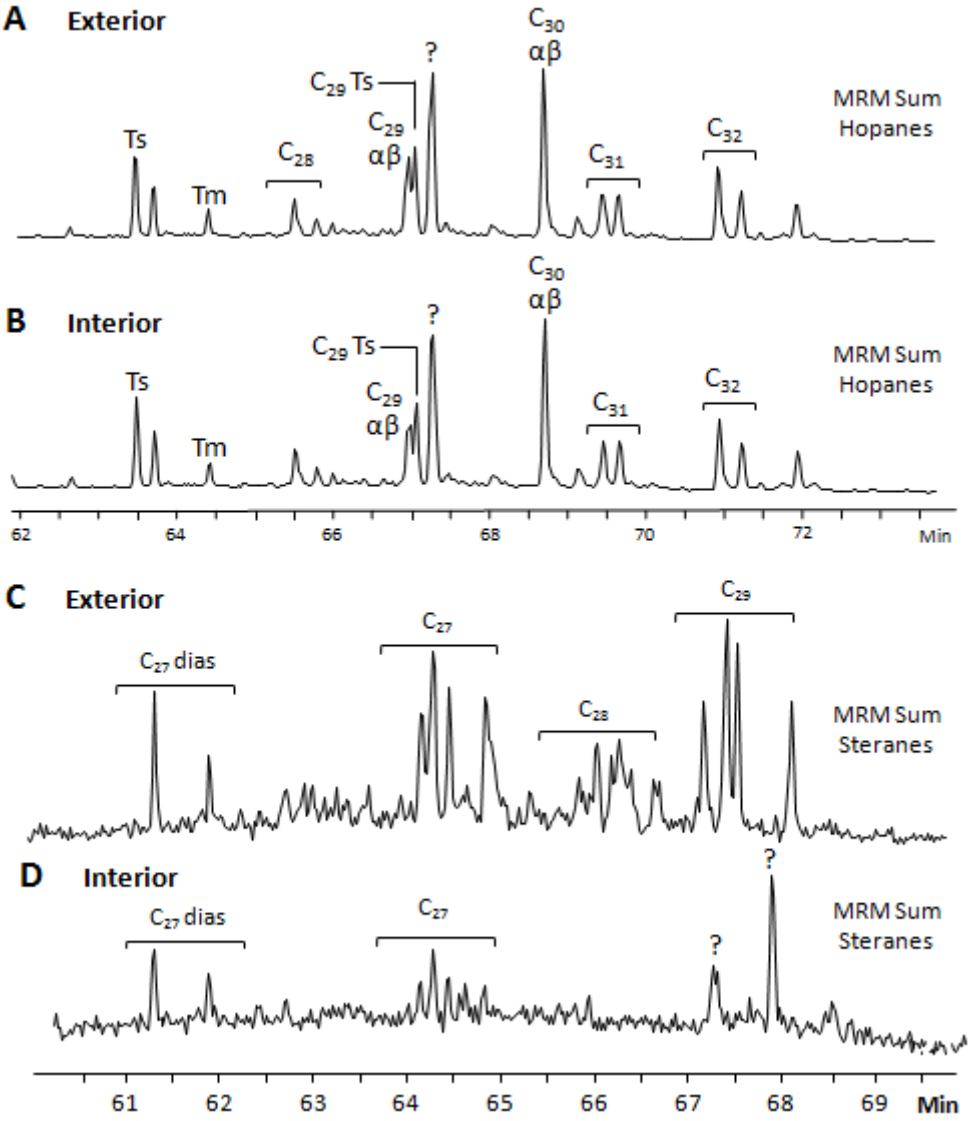

Figure 4. Results of micro-ablation of 471.50 m, drill core BR05DD01. **A-** Shows the summed MRM traces of C_{27} – C_{31} regular hopanes (370, 384, 398, 412, 426 → 191) in the saturated hydrocarbon fraction of the exterior, and **B-** interior. **C-** Shows the summed MRM traces of C_{27} – C_{29} steranes (372, 386, 400 → 217) in the saturated hydrocarbon fraction of the exterior, and **D-** interior. Signal heights in **A** to **D** are approximately proportional to concentrations per gram of rock.

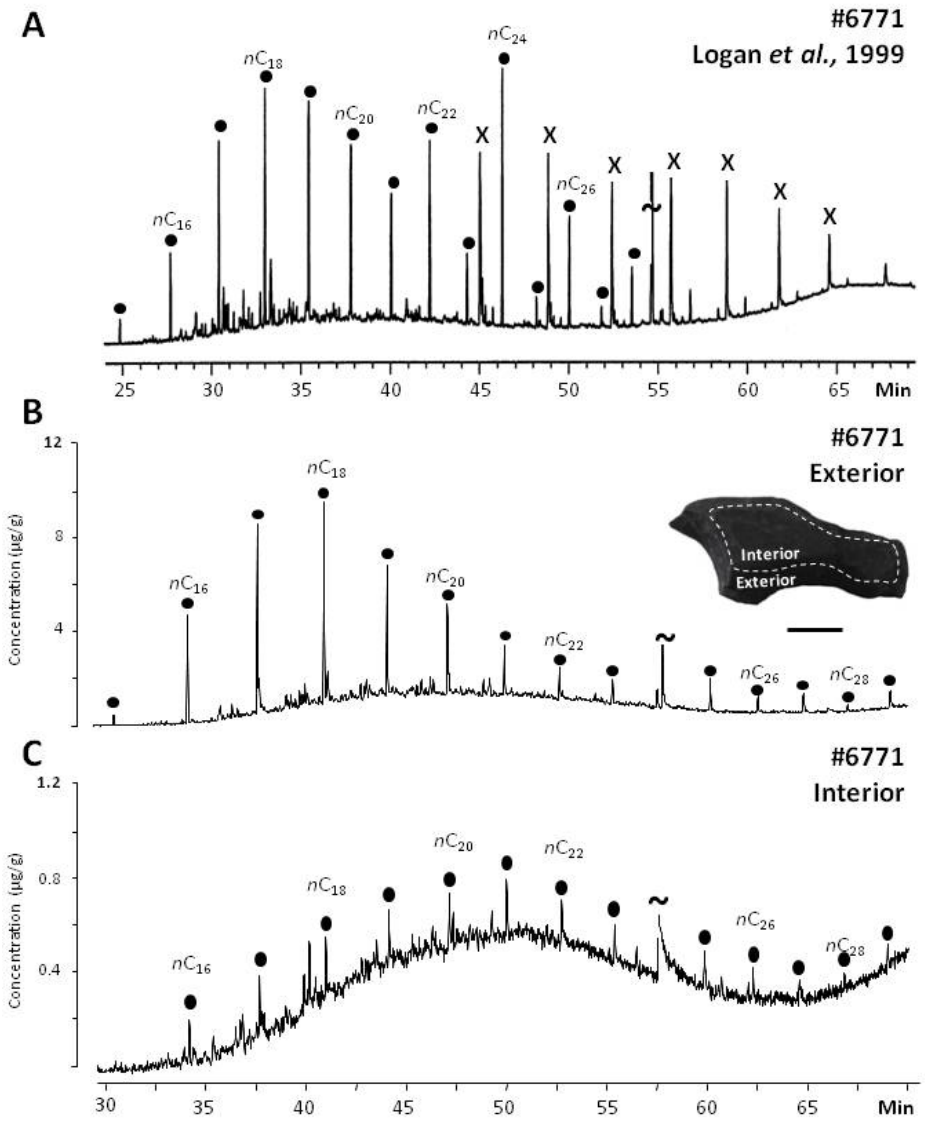

Figure 5. Hydrocarbons from the *ca.* 0.635 Ga Pertatataka Formation, Amadeus Basin (1171.42 m, Wallara-1). **A-** The original full scan chromatogram of the saturated hydrocarbon fraction taken from Logan *et al.* (1999) (Sample # 6771). **B-** GC-MS total ion current of the saturated hydrocarbon fraction of the exterior and **C-** the interior of the re-analysed sample. Signal heights in B and C are scaled to absolute concentrations (per gram of extracted rock). Filled circles represent *n*-alkanes, 'X' the X-compounds and '~' truncates the internal standard, 18-MEAME. Scale bar is 1 cm.

We have identified 16 out of the 44 samples in BR05DD01 and all eight samples analysed in Wallara-1 as contaminated in both the interior and exterior, and excluded from further interpretations. Our results are similar to detailed exterior/interior experiments on

equivalent GM samples reanalysed by Schinteie (2011) from the Mt Charlotte-1 drillcore (e.g. 1654 m; Logan *et al.* 1997). C_{26} – C_{30} regular and methylated steranes, as well as dinosterane, oleanane and bicadinane were all present on exterior surfaces of the drillcore, and were either below detection limits in the interior, or strongly enriched on the exterior (Schinteie, 2011).

Therefore, the steranes described by Summons & Powell (1991) likely reflect an overprint of anthropogenic molecules, likely drilling fluids derived from Phanerozoic marine oils. Plant triterpenoids are a clear indication of Cretaceous or younger contaminants and have been identified on the surfaces of many drillcores in the Amadeus Basin, and the larger Centralian Superbasin (Jarrett *et al.* 2013). Moreover, plant triterpenoids were present in a layer of dust blanketing drillcore BR05DD01, Ooramina-1 and Wallara-1 in the NTGS drillcore library providing an additional source of contamination.

The pervasiveness of contamination of Precambrian drillcore material has only recently been recognised (e.g. Brocks *et al.* 2008; Jarrett *et al.* 2013). In particular, steranes are easily compromised due to their low indigenous content in Precambrian rocks. Therefore, without comprehensive exterior/interior assessments of drillcore we cannot be confident about the syngeneity of individual biomarkers (Brocks *et al.* 2008). The BSF generally has low TOC and any indigenous HCs therefore can be easily masked by trace amounts of contaminant HCs (Brocks *et al.* 2008; Jarrett *et al.* 2013). Without evidence to the contrary, previous biomarker evidence e.g. for5 steranes should be regarded as petroleum-based contaminants. To err on the side of caution, the interpretation of biomarkers from the BSF should only be based on samples where exterior/interior experiments have been conducted (e.g. Schinteie, 2011).

3.3 Indigenous steranes in the Amadeus Basin

Seven samples from the shale unit in BR05DD01, including the oil bleed and 17 rocks from the Bitter Springs Formation in BR05DD01 do not contain BAQCs in the interior fractions and have CP-CPI ratios ≈ 1 indicating that 24 samples were relatively well sealed against HC infiltration (Brocks *et al.* 2008). The results of these 24 rocks were used to determine the

biomarker distribution of the Amadeus Basin in the Aralka and Bitter Springs Formation respectively.

The oil bleed contains trace concentrations of C_{26} (< 0.1 ng/g) and low concentrations (0.6 ng/g) of C_{27} steranes. These molecules are not found in the laboratory blanks and are therefore considered to be indigenous HCs. The C_{28}-C_{30} pseudo homologues are below detection limits (Figure 6). Steranes were also identified in all shale samples. As with the oil bleed, C_{27} is the dominant sterane with traces of C_{26} detected and C_{28}-C_{30} below detection limits (Appendix 5). Steranes are below detection limits in the LCM (Figure 8; Appendix 5). C_{26} and C_{27} steranes are detected in the JCM of the BSF (Appendix 5). Significantly however, C_{28} to C_{30} steranes are below detection limits. Although steranes are detectable in the JCM, absolute concentrations of steranes are low, with C_{27} ranging from 0.03 to 1.2 ng/g rock. In addition, sterane / (sterane + hopane) ratios are low ranging from 0.3 to 1.5% (Appendix 5).

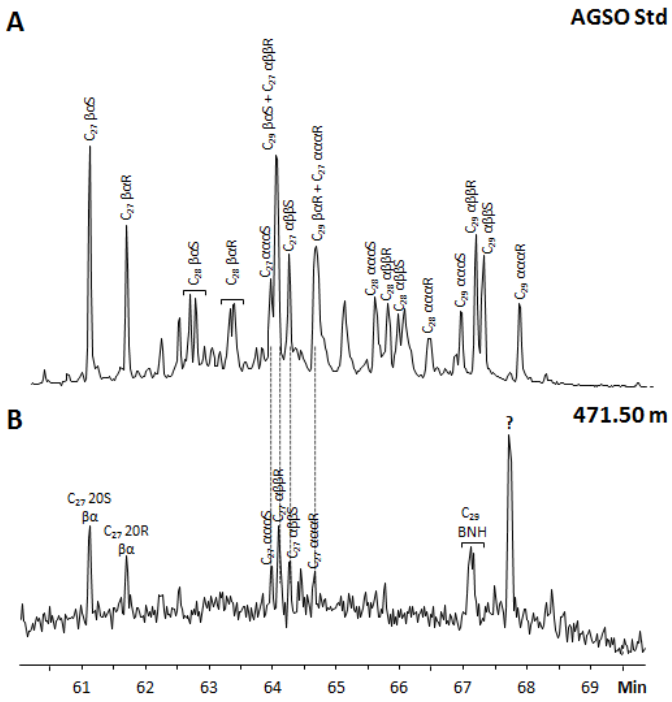

Figure 6. Summed MRM traces of C_{27} to C_{29} steranes (372, 386, 400 → 217) in the saturated hydrocarbon fraction of **A-** the AGSO standard and **B-** the shale at 471.50 m, BR05DD01. C_{29} BNH = C_{29} bisnorhopane.

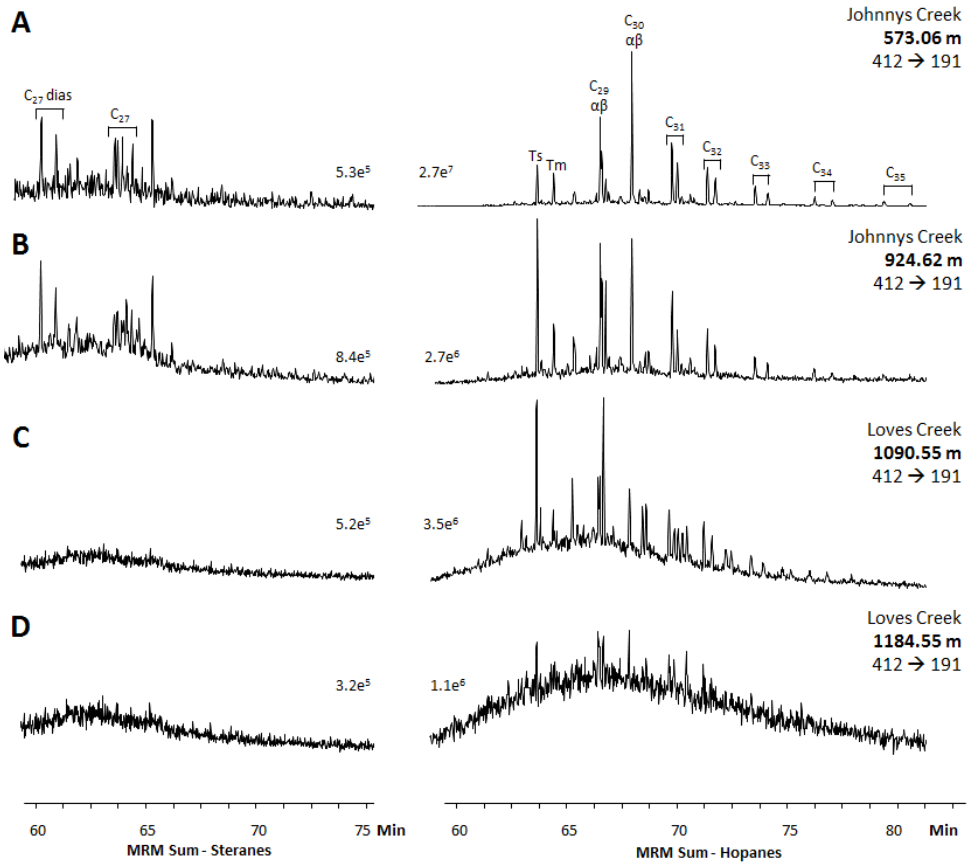

Figure 7. Intensity differences of steranes and hopanes in the BSF. Left panel shows the summed MRM traces of C_{27} - C_{29} steranes (372, 386, 400 → 217) and the right panel shows the summed MRM traces of C_{27} - C_{35} hopanes (370, 384, 398, 412, 426, 440, 468, 482 → 191) in the saturated hydrocarbon fraction of **A-** 573.06 m, **B-** 924.62 m, **C-** 1090.55 m, and **D-** 1224.27 m.

To determine whether the apparent absence of steranes in the LCM is simply caused by an increase in thermal maturity down core, signal/noise (S/N) ratios were calculated using the formula described by Poole (2012);

$$\text{Signal/Noise(S/N)} = \frac{2\text{H}}{\lambda}$$

Where H is the height of the peak of the signal (Figure 8) and λ is the range of the background noise in the chromatogram in the area surrounding the signal peak (Figure 8). S/N for C_{27} steranes, C_{30} αβ-hopanes and gammacerane are presented in Table 2.

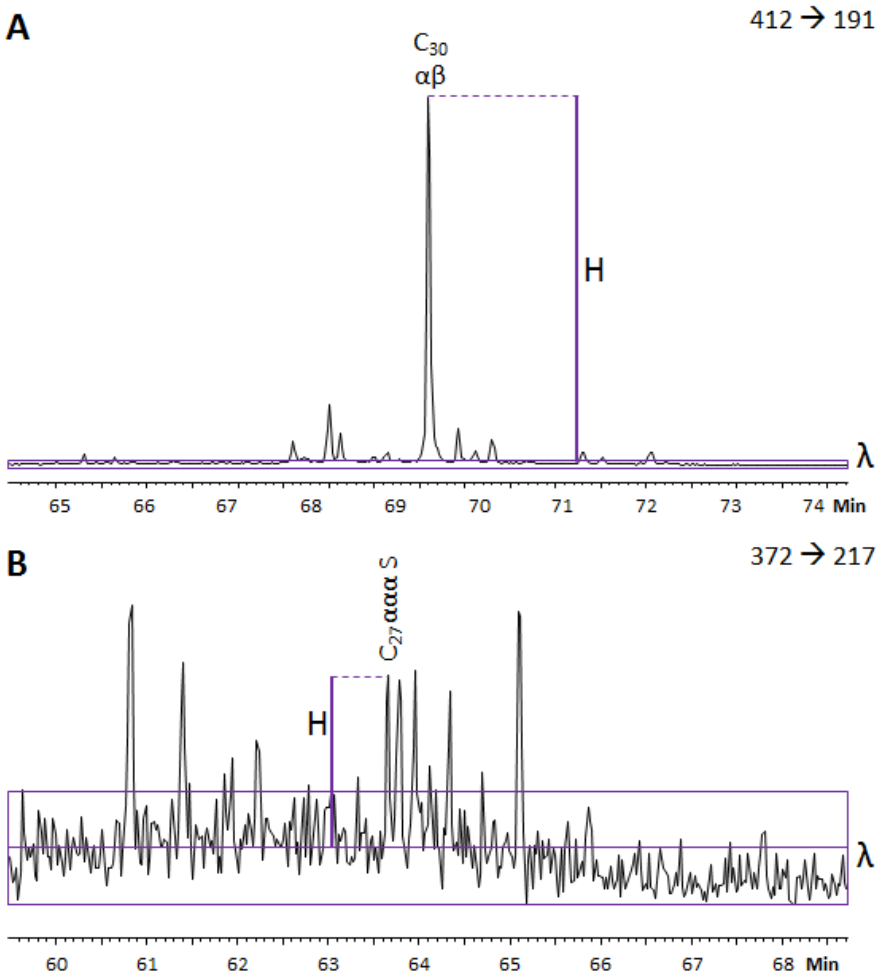

Figure 8. Calculation of signal/noise ratio for **A-** C_{30} αβ- hopane in MRM trace 412 → 191 and **B-** C_{27} ααα S in MRM trace 372 → 217 in sample 573.06 m.

The results in Table 2 demonstrate that in the JCM S/N is higher for C_{30} hopanes (average 232) compared with steranes and gammacerane (averages 4.0 and 17.6, respectively) by one to two orders of magnitude. For 816.26 and 924.62 m, even the least abundant hopane, C_{35}, is three times higher in concentration than C_{27} ααα S, highlighting the scarcity of steranes. According to the low hopane S/N in the LCM, steranes would not be detected even if their initial concentrations were equivalent to the JCM. However, it is also currently impossible to discount a primary absence of steranes. Without additional samples with a higher hopane S/N it is impossible to assess whether indigenous steranes were present in the LCM. What is apparent, however is that in the JCM the sterane/(sterane + hopane) ratio ranges from 0.29 to 1.5% indicating steranes were only a minor component of the biomass. Eukaryote contribution in the LCM must have been equally low or lower.

Table 2. Signal to noise ratios for C_{27} ααα S sterane, C_{30} αβ hopane and gammacerane (γ) for BSF samples in drillcore BR05DD01

Depth	Formation	C_{27} ααα S	C_{30} αβ	γ
573.06	JCM	3.7	380	13
585.20		4.1	350	64
762.18		3.6	160	10
808.20		8.1	410	43
813.60		3.2	130	3.0
816.26		5.2	550	16
924.62		n.d.	180	11
931.33		3.1	190	20
942.70		2.7	80	4.3
956.07		3.0	87	5.0
961.91		2.9	35	4.8
1090.55	LCM	n.d.	17	8.6
1091.70		n.d.	14	8.3
1106.70		n.d.	21	29
1132.50		n.d.	4.3	3.2
1184.55		n.d.	15	2.5
1224.07		n.d.	22	3.5

A biomarker assemblage composed entirely of cholestane without any higher C_{28} – C_{30} pseudo homologues is a unique pattern, currently known from the pre-Ediacaran. A lack of > C_{27} steranes suggests a low eukaryotic diversity at the time of deposition. However, the source of cholestane remains largely obscure. It has been readily assumed that the C_{27} dominance in the Neoproterozoic is sourced from red algae (e.g. Grantham, 1986; Summons *et al.* 1988; Elie *et al.* 2007). This is primarily due to modern red algae having a high proportion of cholestane in their membranes (Kodner *et al.* 2008). The identification of *Bangiomorpha* in 1.2 Ga sediments also confirms the likelihood of red algae inhabiting Neoproterozoic environments (Butterfield, 2000).

This trend of cholestane predominance continues in the Aralka Formation. However, due to thermal destruction and pervasive contamination it is unclear whether this sterane pattern continues in the Ediacaran Pertatataka Formation. However, C_{29} predominance appears to be a prevalent and unique signature of the Ediacaran also observed in contemporaneous oils and organic rich facies from Oman, the Eastern European Platform and Western India

(Grosjean *et al.* 2009; Fowler and Douglas 1987; Bazhenova and Arefiev 1996; McKirdy *et al.* 2006; Dutta *et al.* 2013).

3.4 Relationships between oxygen and evolution

The results of this study indicate that the Ediacaran water column in the Amadeus Basin was oxygenated immediately preceding the Marinoan Glaciation. Although there is no current indigenous Ediacaran biomarker record in the Amadeus Basin, microfossil evidence suggests that eukaryotes were not radiating co-eval with oxygenation (Grey, 2005), however it is possible these results may be skewed due to preservation bias.

Thus, unlike other localities such as South China or the Eastern European Platform (Johnston *et al.* 2010; Sahoo *et al.* 2012), the appearance of pervasive oxygen does not correlate with diverse eukaryote fossils such as large colonial algae or bilaterians. Although the sediments analysed provide a patchy resolution of biomarkers through the Basin, the results indicate that eukaryotes are not a dominant part of the biomass in the Amadeus Basin, even after oxygenation.

4. Future Work

As indigenous biomarkers from the Pertatataka Formation were not detected in this study, future work could consist of screening more cores which capture this crucial time interval. The results of this study could also feed into a larger study analysing the petroleum potential, or biomarker study of the entire Amadeus Basin.

Acknowledgements

We would like to thank Simon W. Poulton (University of Leeds) for collaboration with Fe speciation and redox chemistry. Furthermore, we would like to thank Liz Webber (Geoscience Australia), Jun Park Woo (ANU) and Jeremy Wykes (ANU) for assistance in the XRF/ICP-MS laboratory and Janet Hope (ANU) and Zoe Hearne (ANU) for assistance in the Organic Geochemistry laboratory.

5. References

Bazhenova OK, Arefiev OA (1996) Geochemical peculiarities of Pre-Cambrian source rocks in the East European Platform. Organic Geochemistry 25, 341-351.

Brocks JJ (2011) Millimeter-scale concentration gradients of hydrocarbons in Archean shales: Live-oil escape or fingerprint of contamination? Geochimica et Cosmochimica Acta 75, 3196-3213.

Brocks JJ, Buick R, Logan GA, Summons RE (2003) Composition and syngeneity of molecular fossils from the 2.78 to 2.45 billion-year-old Mount Bruce Supergroup, Pilbara Craton, Western Australia. Geochimica et Cosmochimica Acta 67, 4289-4319.

Brocks JJ, Grosjean E, Logan GA (2008) Assessing biomarker syngeneity using branched alkanes with quaternary carbon (BAQCs) and other plastic contaminants. Geochimica et Cosmochimica Acta 72, 871-888.

Butterfield NJ (2000) Bangiomorpha pubescens n. gen., n. sp.: implications for the evolution of sex, multicellularity, and the Mesoproterozoic/Neoproterozoic radiation of eukaryotes. Paleobiology 26, 386-404.

Canfield DE, Poulton SW, Knoll AH, Narbonne GM, Ross G, Goldberg T, Strauss H (2008) Ferruginous Conditions Dominated Later Neoproterozoic Deep-Water Chemistry. Science 321(5891), 949-952.

Canfield DE and Raiswell R (1999) The evolution of the sulfur cycle. Am J Sci 299(7-9), 697-723.

Canfield DE, Raiswell R, Westrich JT, Reaves CM, Berner RA (1986) The Use of Chromium Reduction in the Analysis of Reduced Inorganic Sulfur in Sediments and Shales. Chemical Geology 54, 149-155.

Dutta S, Bhattacharya S, Raju SV (2013) Biomarker signatures from Neoproterozoic-Early Cambrian oil, western India. Organic Geochemistry 56, 68-80.

Fowler MG, Douglas AG (1987) Saturated hydrocarbon biomarkers in oils of Late Precambrian age from Eastern Siberia. Organic Geochemistry 11, 201-213.

Grey K (2005) Ediacaran palynology of Australia. Memoirs of Association of Australasian Palaeontologists 31, 1-43.

Grosjean E, Logan GA (2007) Incorporation of organic contaminants into geochemical samples and an assessment of potential sources: Examples from Geoscience Australia marine survey S282. Organic Geochemistry 38, 853-869.

Grosjean E, Love GD, Stalvies C, Fike DA, Summons RE (2009) Origin of petroleum in the Neoproterozoic-Cambrian South Oman Salt Basin. Organic Geochemistry 40, 87-110.

Hoffman PF, Kaufman AJ, Halverson GP, Schrag DP (1998) A Neoproterozoic Snowball Earth. Science 281(5381), 1342-1346.

Jackson KS, McKirdy DM, Deckelman JA (1984) Hydrocarbon Generation in the Amadeus Basin, Central Australia. Australian Petroleum Exploration Association 2410, 12.

Jarrett AJM, Schinteie R, Hope JM, Brocks JJ (2013) Micro-ablation, a new technique to remove drilling fluids and other contaminants from fragmented and fissile rock material. Organic Geochemistry 61, 57-66.

Kodner RB, Pearson A, Summons RE, Knoll AH (2008) Sterols in red and green algae: quantification, phylogeny, and relevance for the interpretation of geologic steranes, pp. 411-420. Blackwell Publishing Ltd.

Logan GA, Summons RE, Hayes JM (1997) An isotopic biogeochemical study of Neoproterozoic and early Cambrian sediments from the Centralian Superbasin, Australia. Geochimica et Cosmochimica Acta 61, 5391-5409.

Lyons TW and Severmann S (2006) A critical look at iron paleoredox proxies: New insights from modern euxinic marine basins. Geochimica et Cosmochimica Acta 70(23), 5698-5722.

Marshall TN, Dyson IA, Liu K (2008) Petroleum Systems in the Amadeus Basin, central Australia: Were they all oil prone?

Marynowski L, Pieta M, Janeczec J (2004) Composition and source of polycyclic aromatic compounds in deposited dust from selected sites around the Upper Silesia, Poland. Geological Quarterly 48, 169-180.

McKirdy DM, Webster LJ, Arouri KR, Grey K, Gostin VA (2006) Contrasting sterane signatures in Neoproterozoic marine rocks of Australia before and after the Acraman asteroid impact. Organic Geochemistry 37, 189-207.

Poulton SW and Canfield DE (2005) Development of a sequential extraction procedure for iron: implications for iron partitioning in continentally derived particulates. Chemical Geology 214(3-4), 209-221.

Rogge WF, Medeiros PM, Simoneit BRT (2006) Organic marker compounds for surface soil and fugitive dust from open lot dairies and cattle feedlots. Atmospheric Environment 40, 27-49.

Rogge WF, Hildemann, LM, Mazurek MA, Cass, GR, Simoneit, BRT (1993) Sources of fine organic aerosol. 3. Road dust, tire debris, and organometallic brake lining dust: roads as sources and sinks. Environmental Science & Technology 27, 1892-1904.

Schinteie R (2011) Ancient Life at the Extremes: Molecular Fossils and Paleoenvironmental Contexts of Neoproterozoic and Cambrian Hypersaline Settings Australian National University, Canberra, ACT.

Shields-Zhou GA and Och LM (2011) The case for a Neoproterozoic Oxygenation Event: Geochemical evidence and biological consequences. GSA Today 21(3), 4-11.

Summons RE, Powell TG (1991) Petroleum source rocks of the Amadeus Basin, in: Korsch RJ and Kennard JM (Ed.) Geological and Geophysical Studies in the Amadeus Basin, Central Australia. Bureau of Mineral Resources, Australia, Bulletin, 511-524.

Appendix 1- Fe speciation data for drillcore Wallara-1

Depth (m)	Formation	Fe_T	Fe_{HR} / Fe_T [a]	Fe_{Py} / Fe_{HR} [b]	Fe_{Carb} / Fe_T	Fe_{Mag} / Fe_T	Fe_{Ox} / Fe_T
770.36	Pertatataka	4.13	0.18	0.16	0.05	0.05	0.05
826.06		4.28	0.23	0.31	0.06	0.05	0.06
828.06		4.31	0.23	0.38	0.06	0.05	0.04
904.85		2.97	0.18	0.13	0.07	0.04	0.04
1003.45		4.34	0.21	0.13	0.08	0.06	0.04
1060.49		4.62	0.19	0.04	0.07	0.05	0.06
1112.68		6.18	0.21	0.37	0.06	0.05	0.02
1171.26		6.01	0.20	0.00	0.12	0.05	0.03
1202.51		4.69	0.18	0.24	0.06	0.06	0.02
1246.45		3.45	0.15	0.07	0.08	0.05	0.02
1248.18		5.42	0.31	0.00	0.07	0.08	0.15
1276.4	Pioneer	1.80	0.45	0.02	0.39	0.03	0.02
1277.98		2.22	0.37	0.09	0.28	0.03	0.02
1278.54		2.93	0.52	0.09	0.41	0.05	0.02
1278.8		2.72	0.19	0.10	0.12	0.03	0.02
1280.99		2.51	0.30	0.31	0.17	0.03	0.02
1281.93	Aralka	3.21	0.17	0.04	0.08	0.06	0.02
1282.85		3.88	1.04	0.18	0.81	0.02	0.01
1283.1		4.05	0.66	0.48	0.28	0.04	0.02
1283.87		2.57	0.87	0.41	0.49	0.04	0.02
1285		4.25	0.54	0.62	0.16	0.03	0.01
1285.24		4.17	0.58	0.61	0.18	0.03	0.01
1285.7		4.20	0.55	0.45	0.25	0.04	0.02
1286.63		4.22	0.82	0.42	0.42	0.04	0.02
1287.14		3.54	0.74	0.49	0.33	0.03	0.02
1287.85		4.27	0.64	0.58	0.22	0.03	0.02
1288		3.77	0.91	0.48	0.42	0.04	0.02
1288.53		4.26	0.68	0.47	0.28	0.06	0.02
1289.54		4.38	0.64	0.55	0.23	0.04	0.02
1290.3		4.58	0.69	0.56	0.26	0.03	0.02
1291.77		4.69	0.65	0.58	0.23	0.03	0.02
1298.51		5.17	0.77	0.64	0.23	0.03	0.02
1302.84		4.82	0.53	0.46	0.24	0.03	0.01
1303.62		4.26	0.81	0.49	0.37	0.03	0.02
1305.23		3.02	0.76	0.58	0.29	0.02	0.01
1305.6		2.97	0.93	0.35	0.57	0.02	0.02
1309.9	Areyonga	2.67	0.69	0.39	0.36	0.04	0.02
1317.9		2.13	0.74	0.11	0.61	0.03	0.02
1332.24		1.53	0.79	0.06	0.68	0.03	0.02
1358.48		2.33	0.45	0.14	0.32	0.05	0.03
1412.98		2.69	0.32	0.05	0.21	0.07	0.03

Appendix 1 continued

Depth (m)	Formation	Fe_T	Fe_{HR} / Fe_T	Fe_{Py} / Fe_{HR}	Fe_{Carb} / Fe_T	Fe_{Mag} / Fe_T	Fe_{Ox} / Fe_T
1430.08	Johnnys Creek Member; BSF	1.26	0.87	0.37	0.54	0.01	0.01
1487.13		2.37	1.00	0.24	0.73	0.01	0.02
1536.33		0.92	0.35	0.15	0.27	0.02	0.01
1568.37		0.26	0.97	0.08	0.92	0.01	0.00
1614.63		0.54	0.97	0.18	0.49	0.16	0.15
1616.28		0.24	0.96	0.14	0.75	0.05	0.04
1628.87		1.54	0.29	0.15	0.17	0.04	0.04
1657.65		0.22	0.99	0.04	0.88	0.02	0.06
1727		0.04	0.95	0.62	0.25	0.02	0.21
1732.72		0.07	0.93	0.06	0.65	0.09	0.15
1793.3		0.12	0.93	0.03	0.81	0.04	0.07
1796.4		0.05	0.82	0.26	0.45	0.05	0.18
1826.73	Loves Creek Member; BSF	0.71	0.73	0.45	0.35	0.02	0.02
1843.27		0.34	0.95	0.37	0.57	0.02	0.02
1861.95		1.61	0.48	0.47	0.18	0.02	0.06
1864.05		0.32	0.96	0.09	0.76	0.03	0.08
1876.16		0.38	0.98	0.17	0.76	0.02	0.02
1887.21		2.16	0.52	0.61	0.17	0.02	0.02
1897.38		0.42	1.00	0.26	0.69	0.02	0.03
1902.37		0.63	0.99	0.52	0.43	0.02	0.02
1915.26		0.39	0.93	0.13	0.61	0.18	0.02
1936.6		0.67	0.35	0.23	0.18	0.04	0.05
1950.54		0.25	0.69	1.01	0.66	0.01	0.02
1976.79		0.38	0.97	0.17	0.79	0.01	0.02
1989.03		0.22	0.80	0.01	0.72	0.03	0.05
1996.67	Gillen Member; BSF	0.04	0.59	0.13	0.47	0.06	0.06
1998.6		0.35	0.95	0.03	0.73	0.01	0.20

a-The ratio of highly reactive Fe (Fe_{HR}) over total Fe (Fe_T).

b- The ratio of pyrite iron (Fe_{Py}) over highly reactive Fe (Fe_{HR}).

Appendix 2. Concentrations of selected TMs in Wallara-1 (ppm)

Depth (m)	Formation	Al	Fe	P	S	V	Mo	U	Fe/Al
770.36	Pertatataka	75000	41800	0.06	24300	117.00	n.m.	n.m.	0.56
828.06		77800	41600	0.06	26400	121.00	n.m.	n.m.	0.53
904.85		49600	29800	0.05	6920	73.00	n.m.	n.m.	0.60
936.00		16000	6810	0.02	4420	33.20	n.m.	n.m.	0.43
1003.45		62000	39700	0.06	6540	87.60	3.41	3.17	0.64
1056.00		96200	46400	0.05	8740	150.00	n.m.	n.m.	0.48
1083.00		88900	47200	0.06	26400	137.00	0.50	3.53	0.53
1152.00		86500	54400	0.07	9920	144.00	0.44	2.88	0.63
1206.00		87100	47700	0.05	43200	141.00	0.62	3.30	0.55
1230.00		79500	53900	0.07	132000	187.00	4.61	5.35	0.68
1246.45		79700	33100	0.07	1150	292.00	n.m.	n.m.	0.42
1280.99	Pioneer	61300	18200	0.07	5720	127.00	n.m.	n.m.	0.30
1285.00	Aralka	67500	41300	0.08	67500	164.00	2.33	3.89	0.61
1288.00		46200	33400	0.08	92500	119.00	2.86	2.79	0.72
1291.77		68200	44500	0.09	71900	170.00	0.98	3.69	0.65
1295.33		70900	45400	0.09	112000	180.00	6.52	4.10	0.64
1297.82		17200	29000	0.06	46400	51.70	n.m.	n.m.	1.69
1298.51		45600	35700	0.08	73400	120.00	n.m.	n.m.	0.78
1300.72		49700	41800	0.07	98000	115.00	4.50	2.43	0.84
1302.00		70900	47400	0.06	65200	159.00	6.21	3.35	0.67
1306.58		57700	23100	0.06	37100	96.60	0.75	2.74	0.40
1306.97		9420	12500	0.01	32100	9.00	0.97	1.03	1.33
1308.41	Areyonga	5810	5980	0.01	8990	21.50	n.m.	n.m.	1.03
1320.35		39600	22100	0.05	7120	61.00	n.m.	n.m.	0.56
1329.85		27700	13700	0.03	5420	31.20	0.46	1.40	0.49
1337.10		29600	15200	0.03	8090	41.60	0.47	1.40	0.51
1345.25		55800	23900	0.05	12200	74.50	0.73	2.94	0.43
1349.10		47300	24200	0.05	11300	81.90	0.62	2.05	0.51
1356.00		48800	24400	0.05	8920	70.40	0.57	2.16	0.50
1360.70		48500	24000	0.07	15300	78.30	0.72	2.51	0.49
1365.40		46900	22600	0.05	10700	75.30	0.53	3.55	0.48
1376.60		14000	9410	0.02	11600	16.50	0.53	4.03	0.67
1387.40		54900	27200	0.06	2100	94.30	19.13	15.13	0.50
1387.00		45000	25900	0.05	3200	77.60	n.m.	n.m.	0.58
1412.98	Bitter Springs	52800	30800	0.05	2000	81.00	4.12	3.90	0.58
1487.13		10200	12500	0.01	11800	19.80	n.m.	n.m.	1.23
1657.65		1510	1520	0.00	32200	9.20	n.m.	n.m.	1.01
1793.30		1450	1000	0.00	244000	7.90	3.24	3.50	0.69
1996.67		3220	1940	0.00	3920	19.90	0.12	0.19	0.60

Appendix 3. Samples analysed, assessment of syngeneity of HCs (BR05DD01)

Depth From (m)	Formation	Sample description	Exterior removal method[a]	Powder extracted (g)	
				Interior	Exterior
59.83	Aralka Formation	Red to brown mudstone	W	6.66	
154.20		Red to brown mudstone	W	10.03	
154.70		Red to brown mudstone	W	11.53	
154.75		Laminated grey-brown mudstone	S	11.07	16.23
159.09		Dark grey stromatolite	S	24.13	22.73
171.45		Grey laminated mudstone	M	27.38	6.11
171.50		Grey laminated mudstone	W	27.35	
186.98		Dark grey stromatolite	W	7.07	
189.48		Dark grey stromatolite	W	10.74	
191.20		Dark grey stromatolite	W	8.19	
196.93		Dark brown to grey mudstone	W	7.18	
196.95		Dark brown to grey mudstone	M	20.76	12.84
242.20		Laminated grey mudstone	S	9.30	10.43
284.10		Dark grey mudstone	W	31.20	
300.05		Massive grey mudstone	S	6.55	16.63
334.00		Massive grey mudstone	W	23.04	
363.53		Massive grey mudstone	W	18.14	
404.15		Massive grey mudstone	M	13.48	9.87
454.25		Massive grey mudstone	M	3.79	12.07
468.56		Medium grey laminated shale	M	9.58	8.15
471.50		Black laminated shale	M	10.48	12.68
476.20		Medium grey laminated shale	M	29.85	11.46
477.50	Oil bleed	Calcite vein with oil bleed	S	6.91	8.75
480.45	Aralka Formation	Medium grey laminated shale	M	23.67	13.73
481.85		Black laminated shale	S	6.17	4.12
483.60		Black laminated shale	S	23.75	6.68
483.95		Dark grey shale	M	6.85	6.24
484.40		Black laminated shale	W	8.89	
532.34	Areyonga	Diamictite, interlayered shale	S	21.00	26.20
538.80		Diamictite, interlayered shale	S	23.80	22.00
541.00		Diamictite, interlayered shale	S	16.30	12.10
573.06	Johnnys Creek Member	Laminated grey carbonate	S	10.51	23.86
586.20		Brown micritic mudstone with cross cutting molar tooth structures	S	21.90	18.50
586.00		Brown- grey carbonate	S	14.00	13.90

BR05DD01 samples analysed continued

Depth From (m)	Formation	Sample description	Exterior removal method	Powder extracted (g)	
				Interior	Exterior
588.10	Johnnys Creek Member	Laminated grey carbonate with cross cutting molar tooth structures	M	19.70	18.20
606.59		Laminated light grey carbonate	S	12.60	16.00
609.95		Laminated light grey to white carbonate	S	10.82	18.95
611.39		Dark brown to grey laminated carbonate/mudstone	W	3.35	
638.65		Light grey to white carbonate with ooids and halite crystals	M	23.00	8.50
668.83		Laminated grey carbonate	M	24.80	6.50
688.00		laminated grey carbonate with cross cutting molar tooth structures	M	16.70	7.00
692.40		Laminated grey carbonate	S	26.5	27.6
709.30		Laminated light grey carbonate	S	16.12	18.00
731.65		Light to medium grey laminated carbonate	M	26.00	9.80
759.45		Laminated grey carbonate with cross cutting molar tooth structures	W	6.39	
762.18		Laminated grey micritic limestone	S	14.07	24.02
773.69		Laminated grey carbonate	S	13.75	12.25
776.88		Laminated green to grey carbonate	S	14.85	12.00
793.00		Laminated dark grey carbonate	S	9.50	17.90
802.15		Laminated green to grey carbonate	S	17.09	7.93
808.20		Laminated dolomitic mudstone with molar teeth	S	22.71	26.00
813.60		Dark brown microbial mat in a light grey carbonate matrix	S	10.10	17.80
826.35		Laminated grey carbonate	M	23.32	16.94
827.09		Laminated grey carbonate, desiccation structures	M	19.74	6.88
828.25		Laminated green to grey carbonate	S	12.50	12.90
873.04		Laminated grey carbonate	S	21.50	22.77
892.21		Brown and cream microbial mat	W	1.92	
903.04		Dark grey carbonate with styolite	S	12.40	10.50
903.23		Dark grey carbonate with molar tooth features	M	19.00	6.80
908.75		Dark grey to brown carbonate	S	26.50	26.00
912.50		Dark grey to brown carbonate	M	12.10	16.60
914.00		Dark grey to brown carbonate	M	30.07	6.12
924.62		Microbialite with micrite/sparite lamination	S	7.03	23.33

BR05DD01 samples analysed continued

Depth From (m)	Formation	Sample description	Exterior removal method	Powder extracted (g)	
				Interior	Exterior
924.62	Johnnys Creek Member	Microbialite with micrite/sparite lamination	S	7.03	23.33
931.33		Laminated dark grey carbonate, styolites present	S	11.90	17.30
934.75		Laminated dark brown carbonate	S	22.00	36.00
934.83		Dark grey carbonate with evaporitic layers	M	29.30	6.60
942.74		Laminated dark grey carbonate	S	7.00	23.30
956.07		Laminated dark grey carbonate	S	13.96	9.37
956.25		Dolomitic mudstone with molar tooth structures	S	16.98	20.20
959.00		Laminated dark grey carbonate	W	6.74	
961.91		Laminated grey carbonate	S	12.60	23.38
972.30		Red to grey carbonate	M	26.20	13.00
1006.93	Loves Creek Member	Red brown carbonate/mudstone with halite inclusions	W	3.29	
1041.25		Red to grey carbonate	M	12.30	9.80
1068.78		Laminated grey stromatolitic carbonate	M	6.80	3.20
1090.55		Dolomitic mudstone with molar tooth structures	S	13.82	16.95
1091.74		Dolomitic mudstone with an evaporitic layer and molar tooth stuructures	S	13.68	26.52
1106.62		Laminated brown micritic mudstone, cross bedding and laminations	S	19.76	18.25
1132.50		Dark grey carbonate	S	26.50	13.70
1167.12		Dark grey carbonate	M	9.80	6.40
1184.55		Dark grey stromatolitic carbonate with ooids	S	4.55	8.50
1203.23		Laminated grey carbonate with cross cutting molar tooth structures	M	23.30	4.10
1204.28		Dark brown carbonate with molar structures and microbial mat layers	S	9.40	11.90
1207.23		Digitate stromatolites infilled by micrite	M	13.20	6.90
1218.04		Dark grey stromatolitic carbonate	S	14.61	20.59
1224.69		Grey dolomicrite cross cut by thin white molar tooth structures	S	14.61	20.59

(a) Exterior removal method, W = Whole rock extract. S = Exterior surfaces removed using a diamond wafering saw (Brocks, 2011). M = Exterior surfaces removed using micro-ablation (Jarrett *et al.* 2013).

Depth (m)	BAQCR[a]	CP-CPI[b]	Σ*n*-alkanes[d]	E/I *n*-alkanes[e]	E/I Phen[f]	E/I MP[g]	E/I hopanes[h]	E/I steranes[i]	Summary
154.75									
Exterior	10	2.1	4.81	7.5	∞[k]	∞	∞	∞	**Group I:** Low concentrations of n-alkanes < 1 µg / g rock in I. E/I suggest *n*-alkanes are contaminants.
Interior	n.d.[j]	2.7	0.64						
159.09									
Exterior	51	6.9	3.4	3.3	4.4	3.5	17.6	∞	**Group II:** High BAQCs and CP-CPI in I, sample permeable. High E/I ratios indicate contamination.
Interior	34	6.3	1.04						
171.45									
Exterior	10	4.0	21.9	52.1	4.6	8.2	42	30[L]	**Group II:** High BAQCs and CP-CPI in I, sample permeable. High E/I ratios indicate contamination.
Interior	10	3.7	0.42						
196.95									
Exterior	40	6.0	1.95	6.4	1.9	1.0	∞	∞	**Group II:** High BAQCs and CP-CPI in I, sample permeable. High E/I ratios indicate contamination. Indigenous aromatics
Interior	21	2.3	0.36						
242.20									
Exterior	25	2.0	6.14	0.7	1.0	1.1	1.2	1.3	**Group III:** Low BAQCs and CP-CPI, sample not permeable. E/I ratios ≈ 1. Indigenous HCs preserved.
Interior	n.d.	0.9	4.31						
300.05									
Exterior	21	2.5	6.98	4.4	6.3	3.3	2.9	∞	**Group II:** BAQCs in I, sample permeable. Elevated E/I ratios indicate contamination.
Interior	3	1.8	1.36						
404.15									
Exterior	19	2.2	3.59	2.6	1.9	1.9	1.6	3.6	**Group II:** High BAQCs, sample permeable. High E/I ratios indicate contamination.
Interior	14	2.2	1.35						
454.25									
Exterior	25	2.0	1.0	∞	0.24	0.28	∞	∞	**Group I:** Low concentrations of n-alkanes < 1 µg / g rock in I. E/I suggest *n*-alkanes are contaminants. Indigenous aromatics
Interior	n.d.	n.d.	n.d.						
468.56									
Exterior	31	3.1	92.3	1.0	0.95	0.95	0.94	1.1	**Group III:** Low BAQCs and CP-CPI in I, sample not permeable. E/I ratios ≈ 1. Indigenous HCs preserved.
Interior	n.d.	1.0	92.4						

Depth (m)	BAQCR[a]	CP-CPI[b]	Σ*n*-alkanes[d]	E/I *n*-alkanes[e]	E/I Phen[f]	E/I MP[g]	E/I hopanes[h]	E/I steranes[i]	Summary
471.50									
Exterior	12	1.9	20.5	0.87	1.1	0.96	0.97	8.1^{L}	**Group III:** Low BAQCs and CP-CPI, sample not permeable. E/I for most HCs ≈ 1. Exterior steranes are surficial contaminants with different $C_{27} - C_{29}$ ratios than I (see text).
Interior	n.d.	1.1	21.2						
476.20									
Exterior	n.d.	1.9	13.9	0.33	0.25	0.28	0.75	0.71	**Group III:** Low CP-CPI, rock not permeable, low E/I = evaporation from exterior and indigenous interior.
Interior	n.d.	1.0	41.4						
477.50									
Oil bleed	n.d.	1.3	342.5	n.m.[M]	n.m.	n.m.	n.m.	n.m.	**Group III:** The outside of the oil bleed was cut with a diamond saw to remove potential contaminants.
480.45									
Exterior	n.d.	1.1	42	0.52	0.5	0.5	0.56	1.1	**Group III:** No PE contamination, low E/I = evaporation from exterior and indigenous interior.
Interior	n.d.	0.9	81.6						
481.85									
Exterior	n.d.	1.0	152.6	0.78	0.99	1.0	0.9	27^{L}	**Group III:** No PE contamination, low E/I = evaporation from exterior and indigenous interior. Steranes surficial contamination.
Interior	n.d.	1.0	194.7						
483.60									
Exterior	n.d.	1.5	327.6	3.8	2.0	1.8	12	11^{L}	**Group II:** High CP-CPI, rock permeable to contaminants. High E/I > 1 for most sat and aroms; contamination.
Interior	n.d.	1.5	86.2						
483.95									
Exterior	20	2	1.71	∞	1.0	0.9	∞	∞	The interior saturate fraction is devoid of HCs (**Group I**), however the aromatic fraction contains **Group III** HCs.
Interior	n.d.	n.d.	n.d.						
573.06									
Exterior	n.d.	0.71	167.5	0.95	0.92	0.82	1.1	1.2	**Group III:** No PE contamination, low E/I = evaporation from exterior and indigenous interior.
Interior	n.d.	0.70	176.3						

Depth (m)	BAQCR[a]	CP-CPI[b]	Σ*n*-alkanes[d]	E/I *n*-alkanes[e]	E/I Phen[f]	E/I MP[g]	E/I hopanes[h]	E/I steranes[i]	Summary
586.20									
Exterior	n.d.	1.0	12.2	0.97	1	0.9	1	1.5	**Group III:** Low BAQCs and CP-CPI in I, sample not permeable. E/I ratios ≈ 1. Indigenous HCs preserved
Interior	n.d.	1.0	12.5						
709.30									
Exterior	65	2.2	3.1	3.1	2.3	4.8	∞	∞	**Group II:** High BAQCs and CP-CPI, sample permeable. High E/I ratios indicate contamination. Steranes and hopanes have not infiltrated into the rock.
Interior	57.5	2.0	1.0						
762.18									
Exterior	n.d.	1.3	89.0	1.03	1.12	0.98	1.07	8.1[L]	**Group III:** Low BAQCs and CP-CPI in I, sample not permeable. E/I ratios ≈ 1. Indigenous HCs preserved
Interior	n.d.	1.0	86.7						
802.15									
Exterior	n.d.	2.7	150.47	4.1	n.d.	n.d.	6.1	8.08[L]	**Group II:** CP-CPI > 1, rock permeated by plastic residue. E/I > 1 contaminated interior.
Interior	n.d.	2.7	36.7						
808.20									
Exterior	n.d.	1.0	62	0.95	0.85	0.97	1.1	1.1	**Group III:** Low BAQCs and CP-CPI in I, sample not permeable. E/I ratios ≈ 1. Indigenous HCs preserved
Interior	n.d.	1.0	64.9						
813.60									
Exterior	n.d.	1.1	72.2	0.82	0.92	0.92	1.3	1.1	**Group III:** Low BAQCs and CP-CPI in I, sample not permeable. E/I ratios ≈ 1. Indigenous HCs preserved
Interior	n.d.	0.96	87.7						
816.26									
Exterior	n.d.	1.3	208.4	0.86	1.08	1.17	1.21	1.45	**Group III:** Low BAQCs and CP-CPI in I, sample not permeable. E/I ratios ≈ 1. Indigenous HCs preserved
Interior	n.d.	0.9	241.2						

Depth (m)	BAQCR[a]	CP-CPI[b]	Σ*n*-alkanes[d]	E/I *n*-alkanes[e]	E/I Phen[f]	E/I MP[g]	E/I hopanes[h]	E/I steranes[i]	Summary
826.35									
Exterior	n.d.	2.1	6.37	5.9	4.61	13.7	∞	∞	**Group II:** CP-CPI > 1, rock permeated by plastic residue. E/I > 1 contaminated interior.
Interior	n.d.	2.1	1.08						
827.09									
Exterior	20	8	3.68	3.2	1.02	1	3.5	∞	**Group II:** High BAQCs and CP-CPI, sample permeable. High E/I ratios for sats indicate contamination. Aroms possibly indigenous.
Interior	5	8.7	1.15						
903.04									
Exterior	80	1.8	6.9	2.84	3.2	3	2.5	3	**Group II:** High BAQCs and CP-CPI, sample permeable. High E/I ratios indicate contamination.
Interior	76	1.8	2.1						
908.75									
Exterior	12	2.1	94.92	2.23	3.5	3.4	∞	∞	**Group II:** High BAQCs and CP-CPI, sample permeable. High E/I ratios indicate contamination. Larger HCs have not infiltrated into the rock.
Interior	10	2.0	42.49						
924.62									
Exterior	23	2.2	174.6	1.5	1.1	1.12	1.6	∞	**Group III:** Elevated BAQCs and low CP-CPI, rock slightly permeable. E/I ≈ 1 largely indigenous interior
Interior	6	1.0	117.3						
931.33									
Exterior	14	1.5	181.9	0.9	1.02	1.09	0.9	0.85	**Group III:** Low BAQCs and CP-CPI, sample not permeable. E/I ≈ 1 indigenous interior
Interior	1	0.9	202.1						

Depth (m)	BAQCR[a]	CP-CPI[b]	Σ*n*-alkanes[d]	E/I *n*-alkanes[e]	E/I Phen[f]	E/I MP[g]	E/I hopanes[h]	E/I steranes[i]	Summary
934.75									
Exterior	10	2.2	6.9	2.56	0.73	0.71	∞	∞	**Group II:** High BAQCs, sample permeable. High E/I ratios for sats indicate contamination. Aroms possibly indigenous.
Interior	5	n.d.	2.3						
934.80									
Exterior	15	1.8	6	∞	0.74	0.5	∞	∞	The interior saturate fraction is devoid of HCs (**Group I**). Aroms possibly indigenous.
Interior	n.d.	n.d.	n.d.						
942.74									
Exterior	6	1.5	54.54	0.51	0.68	0.76	0.73	∞	**Group III:** Low BAQCs and CP-CPI, rock not permeable, low E/I = evaporation from exterior and indigenous interior.
Interior	n.d.	0.96	106.5						
956.07									
Exterior	25	1.9	6.8	1.93	∞	n.d.	∞	∞	**Group II:** High BAQCs and CP-CPI, sample permeable. E/I ratio > 1 for *n*-alkanes, contamination. Other HCs only on surface.
Interior	10	1.8	3						
956.25									
Exterior	28	2.4	142.6	1.45	1.24	1.4	1.3	6.9^{L}	**Group III:** Low BAQCs and CP-CPI inside rock. E/I ≈ 1,, indigenous interior. Exterior steranes are surficial contaminants with different $C_{27} - C_{29}$ ratios than I (see text).
Interior	2	1.0	97.7						
961.91									
Exterior	n.d.	1.0	6.34	0.65	0.63	0.83	0.8	∞	**Group III:** Low CP-CPI, rock not permeable, low E/I = evaporation from exterior and indigenous interior.
Interior	n.d.	1.1	9.75						
1090.55									
Exterior	n.d.	1.0	200	1.19	1	1.1	1	∞	**Group III:** Low CP-CPI, rock not permeable, E/I ≈ 1, indigenous interior
Interior	n.d.	1.0	180						

Depth (m)	BAQCR[a]	CP-CPI[b]	Σ*n*-alkanes[d]	E/I *n*-alkanes[e]	E/I Phen[f]	E/I MP[g]	E/I hopanes[h]	E/I steranes[i]	Summary
1091.74									
Exterior	10	1.2	178.2	0.84	0.6	0.8	0.8	∞	**Group III:** Low CP-CPI, rock not permeable, low E/I = evaporation from exterior and indigenous interior.
Interior	n.d.	1.0	212.1						
1106.62									
Exterior	n.d.	0.99	54.6	0.51	0.61	0.77	0.8	n.d.	**Group III:** Low E/I = evaporation from exterior and indigenous interior.
Interior	n.d.	1.0	106.5						
1132.50									
Exterior	n.d.	1.0	191.8	0.85	0.9	1.1	1.2	∞	**Group III:** E/I ≈ 1, indigenous interior.
Interior	n.d.	1.0	226.6						
1184.55									
Exterior	n.d.	1.2	10.3	0.86	0.9	0.85	0.9	n.d.	**Group III:** E/I ≈ 1, indigenous interior
Interior	n.d.	1.2	11.9						
1204.28									
Exterior	29.7	2.5	21.1	2.65	1.91	2.82	2.4	2.5 [L]	**Group II:** High BAQCs and CP-CPI, sample permeable. High E/I ratios indicate contamination.
Interior	12.7	2.4	7.96						
1218.04									
Exterior	12.7	2.2	357.5	4.23	1.93	1.79	9.3	4.5	**Group II:** High BAQCs and CP-CPI, sample permeable. High E/I ratios indicate contamination for sats. Aroms possible indigenous
Interior	29.6	1.1	84.3						
1224.69									
Exterior	6.7	2.11	79.4	0.62	0.9	0.87	1.4	∞	**Group III:** No BAQCs inside rock and low CP-CPI, rock not permeable, low E/I = evaporation from exterior and indigenous interior.
Interior	n.d.	1.04	124						

Note that 26 samples from BR05DD01 with negligible HCs (*n*-alkane ≤ 1 µg/g rock) in the interior and exterior fractions are omitted from the table.

a- BAQCR = C_{19} 5,5-diethylpentadecane/*n*-C_{18}. Concentrations were estimated using uncorrected signal areas in *m/z* 127 (Brocks *et al.* 2008).
b- CP-CPI = 2 x (C_{16} + C_{18} + C_{20} + C_{22}) / (C_{15} + 2 x (C_{17} + C_{19} + C_{21}) + C_{23}) cyclopentanes.
c- Presence of polychlorinated biphenyls (PCBs).
d- The sum of individual *n*-alkanes from *n*-C_{13} – *n*-C_{32} where applicable.
e- Exterior/interior ratio of individual *n*-alkanes calculated in d.
f- Exterior/interior ratio of the concentration of phenanthrene measured in the *m/z* 178 trace
g- Exterior/interior ratio of the concentration of methyl phenanthrenes measured in the m/z 192 trace.
h- Exterior/interior ratio of the concentration of the sum of αβ- C_{27} to C_{35} hopanes.
i- Exterior/interior ratio of the sum of C_{27}, C_{28} and C_{29} regular steranes (all ααα- and αββ- 20S and R isomers).
j- Not detected.
k- '∞' indicates that the HC was present on the exterior but below detection limits in the interior.
l- These samples contained surficial contamination of steranes, most likely sourced from dust.

There was no 'exterior' fraction of the oil bleed. To remove any potential contaminants, the exterior surfaces of the calcite vein were removed using a solvent cleaned wafering blade

Appendix 4. Samples analysed, assessment of syngeneity of HCs (Wallara-1)

Legend for next page:

a- Exterior removal method S = sawing, M = micro-ablation.

b- BAQCR = C_{19} 5,5-diethylpentadecane/*n*-C_{15}. Concentrations were estimated using uncorrected signal areas in *m/z* 127 (Brocks *et al.,* 2008).

c- CP-CPI = 2 x (C_{16} + C_{18} + C_{20} + C_{22}) / (C_{15} + 2 x (C_{17} + C_{19} + C_{21}) + C_{23}) cyclopentanes.

d- Presence of oleanane or taraxastane in the extract.

e- Presence of polychlorinated biphenyls (PCBs).

f- b.d. = below detection limits.

g- '∞' indicates that the HC was present on the exterior but below detection limits in the interior.

h- Macquarie University numbers from Logan *et al.* (1999).

i- AGSO numbers from Logan *et al.* (1999).

j- AGSO number from Logan *et al.* (2001).

Well	Depth (m)	Literature ID	Rock Mass (g)	Exterior Removal Method[a]	BAQCR[b]	CP-CPI[c]	Triterpanes[d]	PCBs[e]	Σ*n*-alkanes (µg/g)	E/I *n*-alkanes	E/I hopanes	E/I steranes
Wallara-1	**826.06**			S								
	Exterior		20.0		6	2.2	yes	yes	5.0	7.7	5.0	12.2
	Interior		20.4		29	0.9	yes	b.d.[f]	1.0			
	904.85			S								
	Exterior		26.0		30	6.2	yes	yes	2.8	1.9	1.8	1.2
	Interior		16.8		38	5.5	yes	yes	1.4			
	1003.45			M								
	Exterior		30.0		24	6.4	b.d.	yes	5.5	27	b.d.	b.d.
	Interior		33.0		2	2.7	b.d.	b.d	0.2			
	1060.49			M								
	Exterior		21.1		7	2.2	b.d.	yes	0.40	1.0	b.d.	b.d.
	Interior		15.7		1	1.1	b.d.	yes	0.40			
	1112.68			M								
	Exterior		25.6		21	5.9	yes	yes	6.1	3.2	∞[g]	∞
	Interior		14.3		7	0.46	b.d.	yes	1.9			
	1132.80	25.118[h]		M								
	Exterior		15.0		b.d.	0.8	b.d.	yes	5.2	52	∞	∞
	Interior		15.2		b.d.	b.d.	b.d.	yes	0.1			
	1171.42	6771[i]		M								
	Exterior		13.3		22	b.d.	yes	yes	5.4	4.9	∞	∞
	Interior		12.8		12	b.d.	b.d.	b.d.	1.1			
	1177.80[k]	25.105/4[h]		M								
	Exterior		11.2		34	2.7	yes	yes	0.90	9.0	12	b.d.
	Interior		6.1		b.d.	b.d.	b.d.	b.d	0.10			

Continued

Well	Depth (m)	Literature ID	Rock Mass (g)	Exterior Removal Method[a]	BAQCR[b]	CP-CPI[c]	Plant terpenoids[d]	PCBs[e]	Σ*n*-alkanes (µg/g)	E/I *n*-alkanes	E/I hopanes	E/I steranes
Wallara-1	**1181.70**	25.106[i]		M								
	Exterior		14.3		b.d.	1.2	b.d.	yes	1.2	6.0	∞	∞
	Interior		15.4		b.d.	b.d.	b.d.	b.d.	0.2			
	1190.01[k]	25.109/1[h]		M								
	Exterior		19.4		b.d.	b.d.	b.d.	yes	0.50	5.0	∞	∞
	Interior		7.5		b.d.	b.d.	b.d.	b.d.	0.10			
	1202.10[k]	6772[i]		M								
	Exterior		16.7		b.d.	b.d.	b.d.	yes	0.30	3.0	∞	∞
	Interior		16.4		b.d.	b.d.	b.d.	b.d.	0.10			
	1202.55	6774[i]		M								
	Exterior		15.6		17	1.5	b.d.	yes	0.40	2.0	b.d.	b.d.
	Interior		12.0		8	1.1	b.d.	b.d.	0.20			
	1225.50			M								
	Exterior		17.4		b.d.	b.d.	b.d.	yes	0.20	1.0	∞	∞
	Interior		5.8		b.d.	b.d.	b.d.	b.d.	0.20			
	1229.85[k]			M								
	Exterior		11.4		b.d.	1.5	b.d.	yes	1.5	1.9	43	∞
	Interior		12.4		b.d.	b.d.	b.d.	yes	0.8			
	1232.19	25.116[i]		M								
	Exterior		12.5		6	1.5	b.d.	yes	1.9	4.8	∞	∞
	Interior		7.2		b.d.	1.2	b.d.	yes	0.4			

Continued

Well	Depth (m)	Literature ID	Rock Mass (g)	Exterior Removal Method[a]	BAQCR[b]	CP-CPI[c]	Plant terpenoids[d]	PCBs[e]	Σ*n*-alkanes (µg/g)	E/I *n*-alkanes	E/I hopanes	E/I steranes
Wallara-1	**1245.18**			S								
	Exterior		31.6		22	5.2	yes	yes	1.3	10	97.3	84.5
	Interior		35.2		20	b.d.	yes	b.d.	0.1			
	1246.45			S								
	Exterior		27.1		21	6.9	b.d.	yes	2.7	6.8	71.5	∞
	Interior		14.4		b.d.	3	b.d.	b.d.	0.4			
	Interior		35.8		20	1.7	b.d.	b.d.	1.5			

Appendix 5. Biomarker ratios for indigenous hydrocarbons extracted from BR05DD01

A- Calculated vitrinite reflectance equivalent based on the MPDF (Boreham *et al.* 1988). **B-** Pristane/phytane integrated in TIC (Powell & McKirdy, 1973). **C-** Pristane/*n*-C_{17} integrated in TIC (Lijmbach, 1975). **D-** Phytane/*n*-C_{18} integrated in TIC (Lijmbach, 1975). **E-** Steranes/(steranes+hopanes) in %. Steranes were calculated using diasteranes and regular C_{27} ααα (20R + 20S) and αββ (20R + 20S) steranes, C_{28} and C_{29} were below detection. Hopanes were calculated using regular αβ isomers of C_{27} to C_{35} (22R + 22S) (Moldowan *et al.* 1985). **F-** C_{27} diasteranes/(regular ααα 20 (R + S) and αββ 20 (R + S) steranes) (Mello *et al.* 1988). **G-** Sterane ratio 20S/(20S + 20R) for C_{27} steranes (Seifert & Moldowan, 1986). **H-** Ts/(Ts+Tm) (McKirdy *et al.* 1983). **I-** Moretane/(moretane+hopane) ratio = C_{30} βα/(C_{30} βα + C_{30} αβ) (Seifert & Moldowan, 1986). **J-** The hopane ratio C_x 22S/(22R + 22S) (Seifert & Moldowan, 1986). **K-** Hopane ratio = C_{31} αβ (22R + 22S)/C_{30} αβ (22R + 22S) (Seifert & Moldowan, 1980). **L-** C_{30}*/C_{30} ratio (C_{30} αβ diahopane/ C_{30} αβ diahopane + C_{30} αβ hopane) (Li *et al.* 2009). **M-** C_{35} Homohopane index C_{35}/C_{34} αβ hopanes (22S + 22R) (ten Haven *et al.* 1988). **N-** 2α-methylhopane index (C_{30} 2α-methylhopane/ (C_{30} 2α-methylhopane + C_{30} αβ hopane) expressed in % (Summons *et al.* 1999). **O-** 3β-methylhopane index (C_{30} 3β-methylhopane/(C_{30} 3β-methylhopane + C_{30} αβ hopane)) expressed in % (Brocks *et al.* 2003). **P-** Modified gammacerane index (GI*) to include C_{30} diahopane (C_{30}*) GI* = gammacerane/(gammacerane + C_{30} αβ H + C_{30}*) (Sinninghe-Damste *et al.* 1995). **Q-** Tetracyclic polyprenoid ratio TPPr = (2 x TPP Peak A/(2 x TPP Peak A + C_{26} ααα 20R + 20S + αββ 20R & 20S steranes)) (Holba *et al.* 2000). **R-** Dibenzothiophene/phenanthrene integrated in TIC (Hughes *et al.* 1995). n.d. = not detected.

	Shale				Oil bleed	Shale		Johnnys Creek Member										
	242.20	**468.56**	**471.50**	**476.20**	**477.50**	**480.45**	**481.85**	**573.06**	**585.20**	**762.18**	**808.20**	**813.60**	**816.26**	**924.62**	**931.33**	**942.70**	**956.07**	**961.91**
Rc%[A]	0.33	0.48	0.49	0.7	0.73	0.63	0.49	0.4	0.52	0.64	0.63	0.68	0.73	0.49	0.65	0.72	0.64	0.75
Pr/Ph[B]	0.71	1.06	0.63	1.1	0.63	1.3	1.6	1.05	0.91	0.97	1.2	1.3	1.5	1.7	1	0.77	1.1	1.1
Pr/*n*-C_{17}[C]	0.63	0.38	1.5	0.99	2.7	0.8	1.02	0.45	0.34	0.31	1	0.29	0.45	0.5	0.1	0.2	0.15	0.21
Ph/*n*-C_{18}[D]	0.38	0.34	2.7	1.05	5.4	0.63	0.79	0.4	0.34	0.24	0.88	0.27	0.36	0.48	0.12	0.25	0.17	0.21
S/(S+H)%[E]	0.89	0.34	1.9	4	0.9	2.6	4.6	0.29	0.38	0.76	0.81	0.37	0.37	n.d.	1.5	1.3	0.88	1.5
S Dia/Reg[F]	0.17	0.48	0.26	0.81	0.28	0.68	0.36	0.69	0.43	0.51	0.96	1.1	1.1	n.d.	0.65	0.45	0.36	0.88
20 S/(S+R)[G]	0.45	0.46	0.53	0.52	0.46	0.56	0.46	0.47	0.55	0.45	0.45	0.58	0.65	n.d.	0.55	0.58	0.5	0.37
Ts/(Ts + Tm)[H]	0.53	0.9	0.5	0.64	0.77	0.58	0.68	0.59	0.14	0.46	0.71	0.7	0.73	0.54	0.6	0.72	0.74	0.73
M/(M+H)[I]	0.22	0.15	0.08	0.1	0.09	0.08	0.1	0.03	0.07	0.1	0.05	0.05	0.06	0.11	0.07	0.08	0.07	0.06
C_{31} S/(S+R)[J]	0.59	0.59	0.59	0.59	0.6	0.59	0.58	0.59	0.58	0.61	0.6	0.6	0.61	0.57	0.62	0.61	0.58	0.56
C_{32} S/(S+R)[J]	0.58	0.57	0.56	0.56	0.57	0.57	0.57	0.57	0.6	0.58	0.57	0.56	0.13	0.52	0.49	0.58	0.57	0.56
C_{33} S/(S+R)[J]	0.59	0.56	0.58	0.58	0.61	0.6	0.65	0.59	0.6	0.58	0.59	0.61	0.59	0.6	n.d	0.6	0.6	0.55
C_{31}/C_{30}[K]	0.56	0.84	0.69	0.67	0.77	0.7	0.73	0.76	0.97	1.03	0.75	0.82	0.68	0.89	0.58	0.93	0.85	0.92
C_{30}*/C_{30}[L]	0.02	0.07	0.89	0.92	0.84	0.75	0.89	0.14	0.08	0.68	0.71	0.28	0.37	0.46	0.15	0.49	0.42	0.95
C_{35}/C_{34}[M]	0.63	n.d.	0.58	n.d.	0.65	0.49	n.d.	0.63	0.73	0.55	0.55	0.29	0.6	0.23	n.d	0.77	0.66	0.48
2α- MHI[N]	5.1	3.3	2.6	3.3	7.4	1.8	18	1	n.d.	n.d.	n.d.	n.d.	n.d.	n.d.	n.d.	n.d.	1	n.d
3β- MHI[O]	1.1	7.3	3.8	1.7	16	1.6	14.6	6	6	5	5	2	4	n.d	n.d	n.d	1	n.d
GI*[P]	3.3	4.5	4	0.49	5	4	5.1	0.02	0.09	0.04	0.05	0.04	0.02	0.03	0.15	0.03	0.01	0.09
TPP Ratio[Q]	n.d.	0.75	1	0.55	1	0.74	n.d	0.88	0.78	0.78	0.61	n.d	0.73	n.d	n.d	0.62	n.d	n.d
DBT/P[R]	0.3	0.24	0.24	0.43	0.43	0.3	0.45	0.11	n.d	0.77	n.d	0.9	0.21	1	0.93	0.44	n.d	n.d

	Loves Creek Member					
	1090.55	**1091.70**	**1106.70**	**1132.50**	**1184.55**	**1224.07**
Rc%[A]	0.65	0.6	0.46	0.72	0.55	0.72
Pr/Ph[B]	1.05	1.8	1.2	0.7	0.65	0.91
Pr/*n*-C_{17}[C]	0.12	0.18	0.29	0.13	0.09	0.08
Ph/*n*-C_{18}[D]	0.08	0.12	0.38	0.2	0.15	0.11
S/(S+H)%[E]	n.d	n.d	n.d	n.d	n.d	n.d
S Dia/Reg[F]	n.d	n.d	n.d	n.d	n.d	n.d
20 S/(S+R)[G]	n.d	n.d	n.d	n.d	n.d	n.d
Ts/(Ts + Tm)[H]	0.78	0.66	0.59	0.51	0.71	0.77
M/(M+H)[I]	0.06	0.24	0.04	n.d	0.1	0.15
C_{31} S/(S+R)[J]	0.56	0.57	0.59	0.5	0.54	0.56
C_{32} S/(S+R)[J]	0.48	0.52	0.55	n.d	0.7	0.6
C_{33} S/(S+R)[J]	0.51	0.5	0.58	n.d	0.51	n.d
C_{31}/C_{30}[K]	1.19	1.04	1.2	n.d	0.99	0.96
C_{30}*/C_{30}[L]	2.3	0.6	1.5	1.5	2.3	0.62
C_{35}/C_{34}[M]	0.38	n.d	0.8	n.d	n.d	n.d
2α- MHI[N]	n.d	n.d	0	n.d	n.d	n.d
3β- MHI[O]	n.d	n.d	1.5	n.d	n.d	n.d
GI*[P]	0.12	0.34	0.19	0.25	0.05	0.1
TPP Ratio[Q]	n.d	n.d	n.d	n.d	n.d	n.d
DBT/P[R]	n.d	n.d	0.9	0.72	n.d	0.39